Model-independent method for reconstruction of scattering-length-density profiles using neutron or x-ray reflectivity data

Xiao-Lin Zhou and Sow-Hsin Chen
Department of Nuclear Engineering, 24-211, Massachusetts Institute of Technology, Cambridge, Massachusetts 02139
(Received 27 August 1992; revised manuscript received 16 December 1992)

A model-independent method is developed for the reconstruction of the scattering-length-density profile of a film on top of a known substrate or bulk from the measured reflectivity data. The method is first tested on simulated reflectivity data calculated from profiles resembling those used in real experiments. It is shown that the method is effective in faithfully reproducing the original profiles from the simulated data. The method is then tested on experimental data from four different surface films. It is found again that the method is capable of generating physically reasonable profiles whose calculated reflectivities agree to within $\chi^2=1$ with the measured data. In the tests, detailed descriptions are also given for the implementation of the method. Finally, a discussion is given with regard to the application of the method and the precautions needed for using this method.

PACS number(s): 61.12.Bt, 42.25.Gy, 78.66.−w, 61.10.−i

I. INTRODUCTION

X-ray and neutron reflectometry has found numerous applications in the study of condensed-matter and soft-condensed-matter samples. They include liquid surfaces, solid thin films, magnetic materials, surfaces of complex fluids, polymer interfaces, and so on [1]. Though the reflectivity measurement itself turns out to be very simple and efficient, analysis of the reflectivity data remains a difficult task [1,2] because of the lack of a systematic model-independent method which can directly reconstruct a scattering-length-density (SLD) profile from a set of measured reflectivity data [1]. As a result, the reflectometry technique has up to now relied largely on a brute-force least-squares parametric fitting of the data to assumed models. The manual least-squares parametric fitting method works fairly well on some well-understood samples with known profile models [3,4], but it becomes hopeless for other samples when a suitable model is not available. An example is the study of the adhesion on the air-film and film-substrate interfaces by polymers terminated with different functional groups, where the shape of the SLD profiles are not known beforehand, making it impossible to do parametric fitting. Another example is the surface structure of a bicontinuous microemulsion for which the surface structure is unknown [5]. This is especially true when a new unknown physical property about a sample is to be studied. Obviously, the lack of a model-independent method has limited the usefulness of reflectometry to samples with relatively simple surface structures.

Although the inverse theory of reflection such as the Gel'fand-Levitan method and the Marchenko method were developed a long time ago [6–8], these methods do not apply to the data processing of neutron and x-ray reflectivity experiments because they require the reflectance data (containing both modulus and phase), while most reflectometers are capable of measuring the reflectivity data only (without phase). The measurement of the phase of the reflectance is inherently difficult, if not impossible. Its implementation at a reflectometer would mean sizable extra cost and undesirable complexity added to the intrinsically simple and elegant reflectivity technique. Therefore, it seems more advisable to develop a model-independent method which can process the phaseless reflectivity data than to measure the phase so that one can use Marchenko's method.

In this paper we present an alternative model-independent method for the construction of SLD profiles directly from the phaseless reflectivity data. This method applies to reflectance data as well, although it is meant for the phaseless experimental reflectivity data. The arrangement of the paper is as follows: Section II presents two simple examples to illustrate how the scattering-length density of a sample is determined from reflection data. Section III presents a step-by-step development of the new method. Section IV describes the testing of the method using simulated reflectivity data. Section V discusses the testing on real experimental data. Section VI summarizes this paper through a discussion of the nature, validity, applications, and result interpretation of the method.

II. TWO EXAMPLES OF DIRECT DETERMINATION OF SLD FROM REFLECTION DATA

In this section we discuss two simple examples in which the SLD profile can be obtained from the reflectivity data directly. The first example is the determination of the SLD of a bulk medium from reflectivity data. This is useful because in experiments such as x-ray reflectivity study [4], the Fresnel reflection is used to determine the SLD of a substrate. The second example is the determination of the SLD of a uniform layer on top of a known substrate. This is the simplest case of a film on top of a substrate.

A. Determination of the SLD of a bulk medium

The simplest reflection is the famous Fresnel reflection given by

$$r=\frac{k_0-k}{k_0+k}\ , \tag{1}$$

where $k=[k_0^2-4\pi\rho]^{-1/2}$, with ρ denoting the SLD of the bulk medium. If the reflectance r is measured, then the SLD ρ can be expressed as

$$\rho=\frac{k_0^2}{\pi}\frac{r}{(1+r)^2}\ . \tag{2}$$

As expected, ρ can be calculated directly from a single datum of reflectance r at a given $k_0=2\pi\sin\theta/\lambda$, where λ is the wavelength of the probing radiation and θ the angle of the specular reflection. If only the modulus of r is measured (in practice, $|r|^2$), then we find, for real ρ,

$$\rho_{\pm}=\pm\frac{k_0^2}{\pi}\frac{|r|}{(1\pm|r|)^2}\quad(|r|<1)\ , \tag{3}$$

where "+" and "−" correspond to positive ρ and negative ρ, respectively. This is a double degeneracy, meaning that one measured datum $|r|$ at k_0 corresponds to two possible values of ρ, one positive and the other negative. However, there are two ways to determine which sign to choose. One is by preknowledge about the material compositions of the sample. The other is by measuring two data $|r_1|$ and $|r_2|$ at two separate values $k_0=k_1$ and $k_0=k_2$. Then one substitutes the two data into Eq. (3) to obtain four possible values: $\rho_{\pm}^1$ from datum $|r_1|$ and $\rho_{\pm}^2$ from datum $|r_2|$. If one of the two data is measured at small or intermediate k_0, then one of the following two cases will happen: (1) $\rho_+^1=\rho_+^2$ and $\rho_-^1\neq\rho_-^2$ or (2) $\rho_+^1\neq\rho_+^2$ and $\rho_-^1=\rho_-^2$. If the former (1) happens, the correct SLD is $\rho=\rho_+^1=\rho_+^2$, and if (2) happens, then $\rho=\rho_-^1=\rho_-^2$. The reasoning behind this is that the correct SLD should not depend on the value of k_0. An example for this is as follows: Two data $|r_1|=0.1123$ and $|r_2|=0.2378$ of $|r|$ are taken at $k_0=k_1=0.015$ Å^{-1} and $k_0=k_2=0.030$ Å^{-1}. Four values of ρ are calculated from the two data using Eq. (3) to be

$$\rho_+^1=6.50\times10^{-6}\ \text{Å}^{-2}\ ,$$

$$\rho_-^1=-10.2\times10^{-6}\ \text{Å}^{-2}\ ,$$

$$\rho_+^2=6.50\times10^{-6}\ \text{Å}^{-2}\ ,$$

and

$$\rho_-^2=-6.97\times10^{-6}\ \text{Å}^{-2}\ .$$

According to the above argument that ρ does not depend on k_0 and the fact that $\rho_+^1=\rho_+^2$, we determine that the positive sign is the correct sign and the correct SLD is $\rho=6.50\times10^{-6}$ Å^{-2}. This is an example of how the SLD of the simplest sample could be determined from two phaseless data.

It should be pointed out that if both data are taken at large k_1 and k_2, then $|r_1|$ and $|r_2|\ll1$. From Eq. (1) and Eq. (3), it can be shown easily that $\rho_+^1=-\rho_-^1=\rho_+^2=-\rho_-^2$. In this case, the two data are not capable of telling one whether ρ should be positive or negative. In fact, it is not possible to resolve the "±" double degeneracy using any number of data if they are all measured at large values of k_0. This implies that it is the region of small and intermediate values of k_0 that helps to remove the ambiguity due to the absence of phase information in $|r|$.

B. Determination of the SLD of a uniform layer on top of a given substrate

The reflectance of a uniform layer of SLD ρ and thickness d situated on top of a substrate of known SLD ρ_s is given by

$$r=\frac{r_f+r_be^{i2kd}}{1+r_fr_be^{i2kd}}\ , \tag{4}$$

$$r_f=\frac{k_0-k}{k_0+k}\ , \tag{5}$$

$$r_b=\frac{k-k_s}{k+k_s}\ , \tag{6}$$

where $k=[k_0^2-4\pi\rho]^{1/2}$ and $k_s=[k_0^2-4\pi\rho_s]^{1/2}$. If the reflectance r is measured, the SLD of the uniform sample can be expressed as

$$\rho_s=\frac{k_0^2}{\pi}\frac{\alpha}{(1+\alpha)^2}+\left[\frac{1-\alpha}{1+\alpha}\right]^2\rho\ , \tag{7}$$

$$\alpha\equiv\frac{r-r_f}{1-rr_f}e^{-2ikd}\ . \tag{8}$$

Equation (7) is a transcendental equation for ρ and it can be shown that it has a single root. This equation applies to the entire k_0 range. We can partially prove that Eq. (7) has unique solution at least at large k_0. At large k_0, α becomes

$$\alpha\approx\left[r-\frac{\pi\rho}{k_0^2}\right]e^{-2ik_0d}\quad\text{at large } k_0\ , \tag{9}$$

Using Eq. (9), Eq. (7) can be solved for ρ as

$$\rho\approx\frac{\rho_s-\frac{k_0^2}{\pi}\mathbf{r}}{1-e^{-2ik_0d}}\ . \tag{10}$$

The measurement of a single reflectance datum at large k_0 can determine ρ from Eq. (10), which is the special case of the general relation Eq. (7) at large k_0.

In practice, $|r|^2$ is measured. The reflectivity is the squared modulus of Eq. (4). We show that one datum $|r|^2$ cannot determine ρ, but two data can if one of them is at small or intermediate k_0. At large k_0, one can derive

$$|r|^2=\frac{\pi^2[\rho^2+(\rho-\rho_s)^2+2\rho(\rho_s-\rho)\cos(2k_0d)]}{k_0^4}$$

$$\text{at large } k_0\ , \tag{11}$$

and ρ can be expressed as

$$\rho_{\pm}=\frac{\rho_s}{2}\left[1\pm\left[1-2\frac{1-\beta}{1-\cos(2k_0d)}\right]^{1/2}\right], \tag{12}$$

$$\beta\equiv\frac{k_0^4}{\pi^2}\frac{|r|^2}{\rho_s^2} \text{ at large } k_0 , \tag{13}$$

Clearly, $\rho_+=\rho_s-\rho_-$, meaning a datum at large k_0 cannot resolve ρ from $\rho_s-\rho$, a double degeneracy. However, the measurement of an additional datum at small or intermediate k_0 can resolve this degeneracy. Let us discuss how this could be done.

If $\rho=\rho_s$, it reduces to Fresnel reflection and the conclusion was proven in Sec. II A. If $\rho=\rho_s/2$, then Eq. (12) becomes a single solution. So the question rests with the case $\rho\neq\rho_s$ and $\rho\neq\rho_s/2$. For different ρ and $\rho_s-\rho$ in the layer, k would be appreciably different at small and intermediate values of k_0, due to the effect of k in the exponential factor in Eq. (4). This phase factor contains useful information about the magnitude of the SLD of the layer. In contrast, at large k_0, k becomes k_0 in the cosine term in Eq. (11), so the SLD ρ does not affect the phase factor (cosine term) and the datum at large k_0 only contains information about the heights of two steps but does not contain much information about the actual value of the SLD of the layer itself. According to this reasoning, we determine the SLD ρ by the following steps: (1) measure one datum $|r_1|^2$ at one large $k_0=k_1$, and use Eq. (12) to calculate ρ_+ and ρ_-; (2) measure another datum $|r_2|^2$ at a small or intermediate $k_0=k_2$; (3) use Eq. (4) to calculate reflectivities $|r_+|^2$ from ρ_+ and $|r_-|^2$ from ρ_- at the same $k_0=k_2$; and (4) compare these two numbers with the measured datum $|r_2|^2$ and choose either ρ_+ or ρ_- depending on whether $|r_+|^2$ or $|r_-|^2$ agrees better with $|r_2|^2$. This is a fairly simple procedure and we demonstrate it by an example. Suppose one measures a layer of $d=50$ Å and obtains a datum $|r_1|^2=4.54\times10^{-6}$ at $k_0=k_1=0.1$ Å^{-2}. Equation (12) gives

$$\rho_+=4.52\times10^{-6}\ \text{Å}^{-2}$$

and

$$\rho_-=-2.52\times10^{-6}\ \text{Å}^{-2} .$$

Then another datum $|r_2|^2=0.130$ is obtained at a small $k_0=k_2=0.006$ Å^{-1}. Then we calculated the reflectivities of ρ_+ and ρ_-, at $k_0=k_2=0.006$ Å^{-1}, respectively, and find $|r_+|^2=0.130$ and $|r_-|^2=0.126$. By comparing $|r_+|^2$ and $|r_-|^2$ with the measured datum $|r_2|^2$, one sees that $|r_+|^2=|r_2|^2$. This means that ρ_+ is the correct SLD of the uniform layer $=4.52\times10^{-6}$ Å^{-2}. In fact, this is a very faithful reproduction of the correct SLD as compared to the known SLD $\rho=4.50\times10^{-6}$ Å^{-2} which was used to generate the two data $|r_1|^2=4.54\times10^{-6}$ at $k_0=k_1=0.1$ Å^{-1} and $|r_2|^2=0.130$ at $k_0=k_2=0.006$ Å^{-1}.

C. Nonlinearity in reflection

The above examples showed how the reflectivity data at small or intermediate k_0 can be used to resolve the degeneracy in the SLD values calculated from one phaseless reflectivity datum. This was made possible by the existence of nonlinearity in the reflectance-profile relationship. To explain this, it is useful to make a comparison between reflection and diffraction. In conventional diffraction [9], the amplitude of the diffracted wave is proportional to the Fourier transform (FT) of the sample profile, and this is a linear relation typical of a weak scattering. In reflection, at small and intermediate k_0 where the SLD of the film is not negligible compared to k_0^2, the reflectance is not a simple FT of the profile but instead a highly nonlinear function of the profile, as can be appreciated from the Parratt's recurrence relation [10]. It is this nonlinearity that has added to the resolving power of the reflectivity technique. Due to this nonlinearity, the different parts of a SLD profile are not equally important to the measured reflectivity as they are to the diffracted signals in a diffraction experiment. Therefore, a different spatial orientation of the sample with respect to the incident beam will result in a different quality of resolution by a reflectivity measurement of the profile. For example, to neutrons, a structure located at the air-film interface is much more visible than one at the film-substrate interface. This is because, at small or intermediate k_0, the phase and intensity of the wave are drastically changed by the SLD in the front portion of the film before the wave reaches the film-substrate interface, resulting in a weaker illumination of the rear portion of the film than of the front portion of the film. Therefore, when the sample is flipped with respect to the beam, the reflectivity at the small and intermediate k_0 range would change appreciably. This means that the reflectivity can resolve the orientation of the sample. In contrast, in diffraction, the wave number is essentially equal to the free-space wave number k_0 throughout the film, and the wave is in a weak-scattering region such that the incident wave illuminates each part of the film with the same intensity and with a phase linearly related to the spatial coordinates inside the profile. As a result of the linearity, the diffraction intensity from a one-dimensional sample would remain unchanged when the sample is flipped with respect to the incident beam, and consequently diffraction intensity cannot resolve orientation. This explains why the small- and intermediate-Q (or nonlinear) region of a reflectivity curve adds extra resolving power to that curve, as compared to a diffraction intensity curve which does not contain such a nonlinear region.

III. MODEL-INDEPENDENT METHOD FOR CONSTRUCTION OF $\rho(z)$ FROM MEASURED DATA $r(k_0)$ OR $|r(k_0)|^2$

In reflection experiments, either the reflectance r (such as in electromagnetic and acoustic reflection) or the reflectivity $|r|^2$ (such as in neutron and x-ray reflection) is measured as a function of the free-space wave number $k_0=2\pi\sin\theta/\lambda$, with θ denoting the grazing angle of in-

cidence and λ the free-space wavelength of the wave. Suppose M data ${}^{m}\mathcal{D}(k_{0i})$ $(i=1,2,\ldots,M)$ ($\mathcal{D}=r$ or $|r|^2$) are obtained at distinct values k_{0i} $(i=1,2,\ldots,M)$; the task of reflection data processing is to determine in the fullest possible way the SLD profile $\rho(z)$ characterizing the reflecting sample situated on top of a known substrate or bulk medium of SLD ρ_s. Since the measured reflection or reflectivity data, which are considered the raw material for the construction of the SLD profile, are in numerical form and are discrete in k_0, it suffices to know the correct numerical values of $\rho(z_j)$ $(j=1,2,\ldots,N)$ and there is no loss of generality in so doing. In the following, a scheme is described for the determination of $\rho(z_j)$ $(j=1,2,\ldots,N)$ from measured data ${}^{m}\mathcal{D}(k_{0i})$ $(i=1,2,\ldots,M)$.

A. Discretization of SLD profile $\rho(z)$

The sample film is situated on top of a given substrate or bulk medium of SLD ρ_s as depicted in Fig. 1. The region of interest is $z=(-d,0)$ and it is equally divided into N sections, each of which has the same thickness Δ such that $N\Delta=d$. This is referred to as an equal-interval division method in this paper. The SLD within each slice is regarded as a constant equal to the average SLD in that slice, and the number of thin slices N can be anything as long as it is sufficiently large so that the finest structure in the profile can be appropriately represented in accordance with the resolution of the experiments. The continuous profile $\rho(z)$ is now replaced by the discretized version $\bar{\rho}_N=[\rho_1,\rho_2,\ldots,\rho_N]$. Obviously, $\lim_{N\to\infty}\bar{\rho}_N=\rho(z)$.

According to the data processing scheme to be presented, N is chosen to be $N=2^n$ $(n=0,1,2,\ldots)$. It must be stressed that $\rho_1,\rho_2,\ldots,\rho_N$ are not necessarily independent of each other and should not be regarded as N independent unknowns. This means the determination of

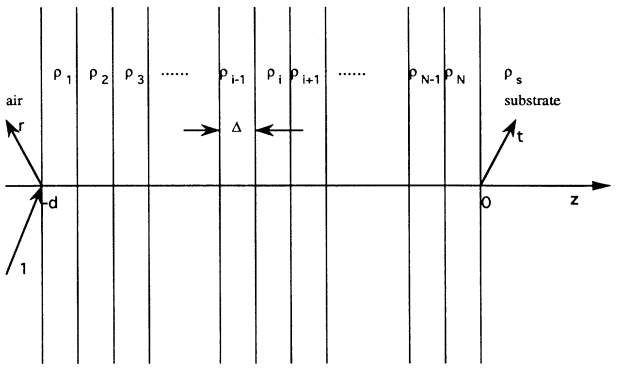

FIG. 1. Geometry of reflection of a plane wave (x-ray or neutron) from a sample film of thickness d situated to the left of the origin of the z axis. The right of the origin $z=0$ is a semi-infinite medium called the substrate or bulk with SLD density ρ_s. The labels "1," "r," and "t" denote the amplitudes of the incident, reflected, and transmitted waves, respectively. The sample is discretized into N slices of equal thickness $\Delta=d/N$. A continuous profile $\rho(z)$ can be accurately represented by the discrete version for sufficiently large N.

$\rho_1,\rho_2,\ldots,\rho_N$ does not necessarily require $N\leq M$. This point will be discussed in more detail in Sec. III B.

The above method of division applies to a region $z=(-d,0)$ in which the functional shape of $\rho(z)$ is totally arbitrary. If there is a region of known SLD profile in the sample, then the SLD profile in that region should be regarded as fixed and is not part of the unknowns to be solved for. Then the sample can be first treated as consisting of three regions: one known region somewhere inside the sample, and two regions with unknown SLD profiles to be found. The above method of equal-interval division should be applied to each of the two regions separately. In general, if there are n_k regions of known SLD profiles and n_u regions of unknown SLD profiles, the equal-interval division method should be applied to each of the n_u regions to discretize each of the n_u unknown profiles, while the SLD profiles of the n_k known regions are fixed. The profile of the entire sample is the combination of the individual subprofiles, and all the unknown subprofiles are to be determined from the measured data jointly by the method given later. This treatment allows the incorporation of preknowledge and constraints on a sample profile.

It should be pointed out that the use of the equal-interval division method is for preserving the model independence of our solution scheme. Any use of unequal-interval division would be equivalent to an assumption about the derivative of the profile (i.e., about how fast a profile varies at different spatial positions). The viability of the use of equal-interval division is guaranteed by the fact that any continuous or discrete profile can be faithfully represented by a discretized profile with equal-interval division as long as N is sufficiently large.

B. Relation between the SLD profile $\bar{\rho}_N$ and the reflection data (r or $|r|^2$)

The solution of the Schrödinger wave equation in the N uniform slices gives the reflectance $r(k_0)$ in terms of the profile $\bar{\rho}_N$ through a recurrence relation [10],

$$r_i=\frac{R_{i+1}+r_{i+1}e^{2ik_{i+1}\Delta_{i+1}}}{1+R_{i+1}r_{i+1}e^{2ik_{i+1}\Delta_{i+1}}} \qquad (i=N-1,N-2,\ldots,2,1,0)\ , \tag{14}$$

where Δ_{i+1} is the thickness of layer $i+1$,

$$k_{i+1}=(k_0^2-4\pi\rho_{i+1})^{1/2}$$

the wave number in layer $i+1$,

$$R_{i+1}=(k_i-k_{i+1})/(k_i+k_{i+1})$$

the Fresnel reflectance of the interface between the layers i and $i+1$, and

$$r_N=(k_N-k_s)/(k_N+k_s)$$

the Fresnel reflectance of the sample-substrate interface. Obviously, r_0 is the reflectance of the entire n-layer assembly, and it is straightforward to calculate r_0 for a given $\bar{\rho}_N$ using Eq. (14). Since a continuous profile can

always be discretized, Eq. (14) is the most efficient method for calculating r and $|r|^2$ of any given $\rho(z)$.

For a given N, r_0 is an analytical function of N variables ρ_i $(i=1,2,\ldots,N)$, though its form becomes complex and highly nonlinear for large N. For convenience, the index "0" is dropped from the N-layer reflectance r_0, and one can write Eq. (14) formally as

$$r(k_0)=P(k_0,\bar{\rho}_N)\ , \tag{15}$$

$$|r(k_0)|^2=|P(k_0,\bar{\rho}_N)|^2\ , \tag{16}$$

where P is an analytical function to be calculated according to the recurrence relation Eq. (14) down to $i=0$. For M ideal data, $\mathcal{D}(k_{0i})$ $(i=1,2,\ldots,M)$ at k_{0i} $(i=1,2,\ldots,M)$, Eq. (15) or Eq. (16) produces M equations of the following form:

$$|\mathcal{D}(k_{0i})-\mathcal{F}(k_{0i},\bar{\rho}_N)|=0 \quad (i=1,2,\ldots,M)\ , \tag{17}$$

where $\mathcal{D}(k_{0i})$ could be either r or $|r|^2$ and $\mathcal{F}$ (which represents a function) could be either P or $|P|^2$ depending on whether r or $|r|^2$ is measured. Equation (17) is an ideal exact equation relating the exact data $\mathcal{D}(k_{0i})$ to the exact SLD profile $\bar{\rho}_N$. Since in practice, the reported data are ${}^m\mathcal{D}(k_{0i})$ $(i=1,2,\ldots,M)$ which are statistical averages with uncertainties $\pm\sigma_i$ $(i=1,2,\ldots,M)$, Eq. (17) can only be satisfied with an uncertainty σ_i if the measured data ${}^m\mathcal{D}(k_{0i})$ are substituted for $\mathcal{D}(k_{0i})$. Therefore,

$$|{}^m\mathcal{D}(k_{0i})-\mathcal{F}(k_{0i},{}^m\bar{\rho}_N)|\le\sigma_i \quad (i=1,2,\ldots,M)\ , \tag{18}$$

where ${}^m\bar{\rho}_N$ is the profile consistently determined from the data ${}^m\mathcal{D}(k_{0i})$. Clearly, when σ_i becomes very small, Eq. (18) approaches Eq. (17). Due to data uncertainties, the profile ${}^m\bar{\rho}_N$ determined from Eq. (18) has uncertainties $\Delta\bar{\rho}_N$. Physically speaking, this means that the reflectivities calculated from ${}^m\bar{\rho}_N$ and that from ${}^m\bar{\rho}_N\pm\Delta\bar{\rho}_N$ differ by an amount of the order of $\pm\sigma_i$; thus, ${}^m\bar{\rho}_N$ and ${}^m\bar{\rho}_N\pm\Delta\bar{\rho}_N$ are undistinguishable by analysis of the M measured reflectivity data. Equation (18) is the equation which relates the measured reflectivity data ${}^m\mathcal{D}(k_{0i})$ [containing errors] to the SLD profile of the sample. It is a set of transcendental equations, the solution of which supposedly will yield ${}^m\bar{\rho}_N$.

However, as often happens, the M equations in Eq. (18) might be mutually inconsistent. The level of inconsistency varies from case to case. The cause may be due to a few sources. First, the normalization of the reflectivity data at the critical edge sometimes is severely affected by the existence of diffuse scattering and other reasons, and a reflectivity curve could be shifted from the actual curve by an amount capable of upsetting Eq. (18). Second, the transverse inhomogeneity existing in the structure of the sample profile may affect the validity of the recurrence relation Eq. (14), which is based on the assumption of the transverse homogeneity, to such a degree that the use of Eq. (14) or Eq. (15) for the calculation of $\mathcal{F}$ in Eq. (18) would result in deviations from Eq. (18) by more than σ_i. Third, residual instrumental errors could also change the relation between the reflectivity data and the sample profiles. Due to these causes, Eq. (18) may not be satisfied perfectly for all experimental cases, but, instead, one may often find that the difference on the left-hand side of Eq. (18) may exceed σ_i or $2\sigma_i$ or $3\sigma_i$ and so on for some values of i. This may severely jeopardize the solubility of Eq. (18) unless it is generalized to allow for the extra deviations due to the above causes. We define an integer inconsistency level $\tau=0,1,2,3,\ldots$, such that a profile ${}_\tau{}^m\bar{\rho}_N$ satisfying

$$|{}_\tau{}^m\mathcal{D}(k_{0i})-\mathcal{F}(k_{0i},{}_\tau{}^m\bar{\rho}_N)|\le\tau\sigma_i \quad (i=1,2,\ldots,M) \tag{19}$$

is called a level-τ profile, meaning that it has an inconsistency level τ. In Eq. (19) the subscript τ of ${}_\tau{}^m\mathcal{D}(k_{0i})$ indicates the level of inconsistency of the data. In this way, when Eq. (18) cannot be satisfied, it will be fine if Eq. (19) is satisfied. Note that $\tau=0$ corresponds to the case of exact data from a perfectly one-dimensional profile. The test profile for a level-τ case is ${}_\tau{}^t\bar{\rho}_N$.

In addition to Eq. (18) and Eq. (19), there is another important relation between the profile ${}^m\bar{\rho}_N$ and the data ${}^m\mathcal{D}(k_{0i})$ $(i=1,2,\ldots,M)$, namely, the relation between M and N. Equations (18) and (19) indicate that there are M equations from M data altogether; thus, the maximum number of independent unknowns determinable from the M equations [Eq. (18)] must not exceed M. However, this does not necessarily mean $N\le M$. For example, Fig. 2 shows a bilayer on top of a known substrate of given ρ_s. The top layer is $\frac{1}{3}$ the thickness of the underlying layer. Obviously, the number of independent unknowns is 2. But according to the method of equal-interval division in Sec. II A, at least four unknowns are needed $(N=4)$ in order to enable the discretized profile to represent the actual profile. Since only two of the four unknowns are independent, two measured data $(M=2)$ are sufficient for the determination of the profile $(\rho_2=\rho_3=\rho_4\neq\rho_1)$, resulting in $N>M$. In general, if the N unknowns are not all independent, it is fine to have $N\ge M$.

C. Outline of scheme for determination of ${}^m\bar{\rho}_N$

The scheme we propose for the determination of ${}_\tau{}^m\bar{\rho}_N$ from the M equations given by Eq. (18) is a scheme of

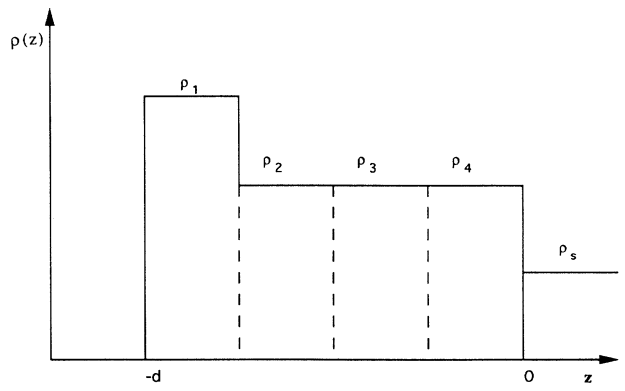

FIG. 2. A bilayer sample containing two independent unknowns requires four $(N=4)$ variables (ρ_1, ρ_2, ρ_3, and ρ_4) for appropriate representation according to the equal-interval division method described in Sec. III A.

motion. This is so because it works in the following way: A test profile ${}_{\tau}{}^{t}\bar{\rho}_N$ at an assumed initial position ${}_{\tau}{}^{0}\bar{\rho}_N$ starts to move in the solution space under the action of a force field which will be defined and explained in Sec. III D. When the test profile reaches a point such that Eq. (19) is satisfied for $i=1,2,\ldots,M$ and the inconsistency level τ cannot be reduced any further, the motion stops and the final test profile ${}_{\tau}{}^{f}\bar{\rho}_N$ coincides with the final solution profile ${}_{\tau}{}^{m}\bar{\rho}_N$, i.e., ${}_{\tau}{}^{f}\bar{\rho}_N={}_{\tau}{}^{m}\bar{\rho}_N$. The two essential parts of this scheme obviously are how to construct the test profile ${}_{\tau}{}^{t}\bar{\rho}_N$ and how to implement its motion. Through numerous tests on simulated reflectivity data, we find it optimum to construct the test profile by a method called the lumped-dimensions method (LD) given in Sec. III D, and the motion of the test profile is most efficiently implemented using the quasi-Newtonian mechanics (QNM) described in Sec. III E.

D. Construction of the test profile by the lumped-dimensions method

When N is very large, such as 1000, the domain of definition of Eq. (19) in the solution space becomes enormous; thus, there are a huge number of possible paths which the test profile could take. Letting the test profile move freely in the domain along an arbitrary path would prove time inefficient as well as susceptible to getting trapped in some corners of the domain. Considering the corresponding monotonic increase in the complexity of the reflectivity curve as the shape of a SLD profile successively increases its complexity to a sequence—single layer, bilayer, quadrilayer, octolayer, etc.—we found that there exists a groove in the domain of Eq. (19) in the solution space and it is possible to make the test profile track this groove systematically provided the test profile is constrained properly. The groove we have found is one along which the motion of a test profile gains complexity monotonically according to the sequence of monolayer, bilayer, quadrilayer, octolayer, etc. To implement the tracking of this groove according to the above sequence, we construct a 2^{ν}-dimensional constrained test profile ${}_{\tau}{}^{t}\bar{\rho}^{\nu}_{2^{\nu}}$ from the N-variable discretized test profile ${}_{\tau}{}^{t}\bar{\rho}_N$. Here $\nu=0,1,2,\ldots,n$, with $2^n=N$. It is apparent that $\nu\le n$ and the equal sign is true at the end of the groove. To obtain 2^{ν} dimensions from N dimensions, we use the lumped dimensions of a lumping ratio $R_{\nu}=N/2^{\nu}$, meaning every R_{ν} dimensions in the total of N dimensions are lumped into one dimension. In this fashion, N dimensions are lumped into 2^{ν} dimensions in an elegant way. As ν changes from 0 to n, R_{ν} takes a sequence of values: $N,N/2,N/4,N/8,\ldots,8,4,2,1$. The so-called groove follows the sequence closely. At $\nu=0$, the lumping ratio is N to 1, meaning that N dimensions are lumped into $2^0=1$ dimension. At $\nu=1$, the lumping ratio is $N/2$ to 1 and the total of N dimensions are lumped into $2^1=2$ dimensions. At $\nu=2$, one has $R_2=N/4$, so every $N/4$ dimensions are lumped into one dimension, and the total of N dimensions turn into $2^2=4$ dimensions. As one approaches the end of the groove, the lumping ratio becomes very small. This is equivalent to saying that the highly lumped dimension of the test profile at the beginning of the groove is delumped gradually until each lump becomes a single dimension in the N-dimensional space for $\nu=n$. Therefore, when a test profile monotonically delumps its dimensions, it is said to be following the groove in the domain of the definition of Eq. (19).

Mathematically, the groove abides by the following delumping sequence, using the notations

$${}_{\tau}{}^{t}\bar{\rho}_N=(\rho_1^n,\rho_2^n,\rho_3^n,\ldots,\rho_N^n)$$

and

$${}_{\tau}{}^{t}\bar{\rho}^{\nu}_{2^{\nu}}=(\rho_1^{\nu},\rho_2^{\nu},\rho_3^{\nu},\ldots,\rho_{2^{\nu}}^{\nu}).$$

(i) $\nu=0$: The test profile ${}_{\tau}{}^{t}\bar{\rho}^{0}_{1}=(\rho_1^0)$ is one dimensional, defined by the N-dimensional lumping

$$\rho_1^n=\rho_2^n=\rho_3^n=\cdots=\rho_N^n\equiv\rho_1^0$$

and this is the starting stage of the groove.

(ii) $\nu=1$: The test profile ${}_{\tau}{}^{t}\bar{\rho}^{1}_{2}=(\rho_1^1,\rho_2^1)$ is two dimensional, obtained by the $N/2$-dimensional lumping

$$\rho_1^n=\rho_2^n=\rho_3^n=\cdots=\rho_{N/2}^n\equiv\rho_1^1$$

and

$$\rho_{N/2+1}^n=\rho_{N/2+2}^n=\rho_{N/2+3}^n=\cdots=\rho_N^n\equiv\rho_2^1\ ,$$

and at this stage, the slope of the profile begins to exhibit itself.

(iii) $\nu=2$: The test profile ${}_{\tau}{}^{t}\bar{\rho}^{2}_{4}=(\rho_1^2,\rho_2^2,\rho_3^2,\rho_4^2)$ is four dimensional, constructed by the $N/4$-dimensional lumping

$$\rho_1^n=\rho_2^n=\rho_3^n=\cdots=\rho_{N/4}^n\equiv\rho_1^2\ ,$$

$$\rho_{N/4+1}^n=\rho_{N/4+2}^n=\rho_{N/4+3}^n=\cdots=\rho_{N/2}^n\equiv\rho_2^2\ ,$$

$$\rho_{N/2+1}^n=\rho_{N/2+2}^n=\cdots=\rho_{3N/4}^n\equiv\rho_3^2\ ,$$

and

$$\rho_{3N/4+1}^n=\rho_{3N/4+2}^n=\cdots=\rho_N^n\equiv\rho_4^2\ .$$

This sequence continues all the way up to the last two members, as follows.

(iv) $\nu=n-1$: The test profile

$${}_{\tau}{}^{t}\rho^{n-1}_{N/2}=(\rho_1^{n-1},\rho_2^{n-1},\ldots,\rho_{N/2}^{n-1})$$

is $N/2$ dimensional, defined by the two-dimensional lumping

$$\rho_1^n=\rho_2^n\equiv\rho_1^{n-1}\ ,$$

$$\rho_3^n=\rho_4^n\equiv\rho_2^{n-1},\ldots,\rho_{N-3}^n=\rho_{N-2}^n\equiv\rho_{N/2-1}^{n-1}\ ,$$

$$\rho_{N-1}^n=\rho_N^n\equiv\rho_{N/2}^{n-1}\ .$$

(v) $\nu=n$: The test profile has dimensions identical to that of the N-variable profile ${}_{\tau}{}^{m}\bar{\rho}_N$. The lumping is one dimensional, or there is no lumping. This is the last member of the sequence and corresponds to the last stage of the groove.

Therefore, the entire groove consists of n stages corresponding to the n members of the above sequence. At each stage, the corresponding test profile moves under the action of a force field resulting from a potential field,

both of which are to be defined in Sec. III E. At an arbitrary stage ν, the potential field and the force field are denoted by $W_\nu(\bar{\rho}^\nu)$ and $\bar{F}_\nu(\bar{\rho}^\nu)$, respectively. Here, $\bar{\rho}^\nu$ is the abbreviation of the test profile ${}_\tau{}^t\bar{\rho}_{2^\nu}^\nu$ at stage ν and this simplified notation will continue to be used in the following discussion for sake of brevity. ${}_\tau{}^t\bar{\rho}_{2^\nu}^\nu$ had been used in previous sections because it was necessary for the discrimination of various quantities when multiple quantities were involved. Note that the test profile constructed through lumped dimensions is sometimes referred to as a lumped test profile in the following sections.

E. Motion of the test profile $\bar{\rho}^\nu$ in the force field $\bar{F}_\nu(\bar{\rho}^\nu)$ generated by Eq. (19)

Once the test profile $\bar{\rho}^\nu$ and the groove of its motion are constructed, it is necessary to specify how it moves. There are two parts to this issue: One is how it moves at a given stage ν of the entire groove. The other is how the test profile makes the transition from a given stage to the next stage when it completes its motion at the given stage. For the first part, the potential field $W_\nu(\bar{\rho}^\nu)$ is first defined and the resulting force field $\bar{F}_\nu(\bar{\rho}^\nu)$ is derived from $W_\nu(\bar{\rho}^\nu)$. With this force field, as will be explained in Sec. III E 2, the implementation uses Newton's law of motion combined with the Monte Carlo sampling method to achieve a motion step. For the second part, the transition of the test profile is made using a continuity condition of the groove or the locus of the test profile in the solution space or the force field. Therefore, the motion of the test profile from the beginning to the end can be summarized in four steps: (1) the test profile at stage $\nu=0$ was placed at an initial position (called initialization) as described in Sec. III E 1; (2) the one-dimensional test profile $\bar{\rho}^0=(\rho_1^0)$ is propelled to move according to the rules prescribed in Sec. III E 2; (3) when it completes this stage $\nu=0$, i.e., when $\bar{\rho}^0$ stops moving, a continuous transition is made to the next stage $\nu=1$, as discussed in Sec. III E 3; (4) the new test profile $\bar{\rho}^1=(\rho_1^1,\rho_2^1)$ is propelled to move in the same way as at step (2) according to Sec. III E 2; and (5) at the end of stage $\nu=1$, a transition is made to stage $\nu=2$ in the same way as in (3). This transition-motion cycle, like the one in steps (2) and (3) or the one in steps (4) and (5), is repeated until $\nu=n$. The basic steps (1), (2), and (3) are detailed in the following sections.

1. *Initialization of* $\bar{\rho}^0$

In the absence of the sample, the reflection should be the simple substrate Fresnel reflection. If the sample has a constant SLD which equals the substrate SLD ρ_s, again the reflection is the simple substrate reflection. If the sample SLD profile $\rho(z)$ is neither zero nor ρ_s, then the reflection becomes different from the substrate Fresnel reflection. The difference directly reflects the SLD profile $\rho(z)$. It then seems very natural to set the initial value of $\bar{\rho}^0$ at either zero or ρ_s.

When the lower and upper bounds of the profile $\rho(z)$ are known beforehand, as is the case in many controlled experiments, one can set $\bar{\rho}^0$ initially to be any value between these two bounds. For example, the average density of the film might be a very wise choice.

In some situations, the sample SLD profiles are some perturbed form of a known functional variation; in that case one can use that known function as the initial condition of a test profile at stage ν_0 provided the test profile has dimensions (different from one dimension) capable of representing the known profile. This is equivalent to skipping the motion of the test profile at stages 0 up to ν_0-1, resulting in saved time.

It is important to know that the scheme to reconstruct the SLD profiles should depend on the initial conditions to the least possible extent. Only in that way can the constructed profiles be called the most objective profiles ever determinable from the measured data. Of course, a constructed profile should always undergo close physical scrutiny before any solid conclusions could be drawn as in the data processing of many other experiments.

2. *Motion of the test profile* $\bar{\rho}^\nu$ *at stage* ν *in the force field* $\bar{F}_\nu(\bar{\rho}^\nu)$

The law of motion described below applies to any step $\nu=1,2,\ldots,n$ along the groove. It is derived from Eq. (19) according to classical Newtonian mechanics. In the derivation, the potential field is constructed first, and the rules of motion of the test profile are then spelled out according to the potential field.

(i) Potential field $W_\nu(\bar{\rho}^\nu)$ *and force field* $\bar{F}_\nu(\bar{\rho}^\nu)$. Equation (19) can be written in a dimensionless form,

$$\left|\frac{{}_\tau{}^m\mathcal{D}(k_{0i})-\mathcal{F}(k_{0i},{}_\tau{}^m\bar{\rho}_N)}{\tau\sigma_i}\right|\le 1 \quad (i=1,2,\ldots,M)\ , \tag{20}$$

the solution of which ${}_\tau{}^m\bar{\rho}_N$ is equal to the final value of the lumped test profile $\bar{\rho}^\nu$ when the test profile reaches the end of the groove. Before the lumped test profile reaches the end point, the substitution of $\bar{\rho}^\nu$ into Eq. (20) for ${}_\tau{}^m\bar{\rho}_N$ would result in the left-hand side of Eq. (20) greater than the right-hand side of Eq. (20). Using this phenomenon, we define M "image particles" which are projections of the test profile in the reciprocal space or k_0 space. These particles are defined to have the following dimensionless potential energies at stage ν:

$$\varepsilon_i^\nu=\left|\frac{{}_\tau{}^m\mathcal{D}(k_{0i})-\mathcal{F}(k_{0i},\bar{\rho}^\nu)}{\tau\sigma_i}\right|-1 \qquad (i=1,2,\ldots,M \text{ and } \nu=0,1,\ldots,n)\ . \tag{21}$$

As the lumped test profile moves from one stage ν down to the next stage $\nu+1$, these particles lose energies. When $\nu=n$, they lose all energies to touch the "ground" at zero potential. Sometimes, they can even fall into the "grass" [meaning the data noise] and stay at a position below the average ground level. In this case, $\varepsilon_i^\nu<0$. When all the M image particles hit the ground of zero potential, the test profile is considered at the ground of a group potential field $W_\nu(\bar{\rho}^\nu)$ defined by

$$W_\nu(\bar{\rho}^\nu)\equiv\frac{1}{M}\sum_{i=1}^{M}\varepsilon_i^\nu\ . \tag{22}$$

This potential field $W_\nu(\bar{\rho}^\nu)$ has a nonvanishing gradient in 2^ν-dimensional space and exerts a force $\bar{F}_\nu(\bar{\rho}^\nu)$ on the lumped profile which moves in it. The force field is simply

$$\bar{F}_\nu(\bar{\rho}^\nu) = -\nabla W_\nu(\bar{\rho}^\nu) \ . \tag{23}$$

Here the gradient operator is with respect to the coordinates $\bar{\rho}^\nu$. This force field determines how the test profile moves along the groove in the solution space, as described in following subsections.

(ii) Scheme of the motion of a lumped profile $\bar{\rho}^\nu$ in $\bar{F}_\nu(\bar{\rho}^\nu)$. The test profile follows the groove discussed in Sec. III D by making a continuous transition to the next stage $\nu+1$ on completing its motion at a previous stage ν. At a given stage ν, it gropes in the force field $\bar{F}_\nu(\bar{\rho}^\nu)$ given by Eq. (23) and moves in the direction of the force according to Newton's law of motion. The force $\bar{F}_\nu(\bar{\rho}^\nu)$ has 2^ν components, and all of them vary as the coordinates $\bar{\rho}^\nu$ change. This means the direction of motion of the test profile changes a lot if one drags the test profile across the domain of definition of $\bar{F}_\nu(\bar{\rho}^\nu)$. However, if we take the average of $\bar{F}_\nu(\bar{\rho}^\nu)$ over its domain of definition, there is usually an average force which points to a certain region of the domain. For example, suppose the domain is divided into two halves A and B and it is found that $W_\nu(\bar{\rho}^\nu)$ is averagely much higher in half A than in half B; there exists a strong average force pointing from half-domain A to half-domain B according to Eq. (23). It may happen that the local force in A sometimes points to a direction away from half-domain B, while that in B points toward A, contrary to the direction of the average force. When the test profile moves in this field, we choose to have the test profile follow the overall direction of the force over the entire domain first before it follows the local variations of the force field in a certain region of the domain. In the above example, even if the test profile starts at an initial position in A and the local force at that point is pointing away from B, we would still like it to move by jumping to B first and then follow the local force in a region B. Once the test profile jumps into B, obviously it can ignore A by scaling down its "leg length" to one-half the dimension of half-space B (note that the largest possible stride of the test profile is equal to twice the leg length).

The above paragraph is just a sketch of the motion scheme we will present. The more detailed and rigorous arguments are as follows: We know that when $\bar{F}_\nu(\bar{\rho}^\nu)$ becomes zero at some positions, the test profile might stop moving. These positions may be either pits or peaks in $W_\nu(\bar{\rho}^\nu)$. The peaks may have different heights from each other, and the pits may have various depths. Only when the test profile reaches the deepest pit can one say the test profile has reached the end of stage ν. As Eqs. (14) and (15) are continuous functions of the profile, the peaks and pits are smooth and well defined and they usually come in smoothly joined pairs. Therefore, the entire domain of definition of $W_\nu(\bar{\rho}^\nu)$ or $\bar{F}_\nu(\bar{\rho}^\nu)$ is characterized by alternating occurrences of peaks and pits in $W_\nu(\bar{\rho}^\nu)$. The domain can thus be divided into many subdomains, each of which correspond to a region including a single pit and the boundary of which is such that a test profile placed at any position inside the subdomain would monotonically move to the bottom of the pit if the test profile exactly follows the direction of the force field $\bar{F}_\nu(\bar{\rho}^\nu)$ in that subdomain. Then the motion scheme of the lumped test profile consists of two steps: (1) jumping into a pit and (2) reaching the bottom of that pit. These two steps are repeated until it can no longer jump or move. At this point, stage ν of the groove is considered completed and the test profile is ready to start the next stage $\nu+1$. This might seem formidably time consuming, but in fact it is not. The major reason is that the lumped dimensions greatly simplify the structure of $W_\nu(\bar{\rho}^\nu)=$const. For example, at $\nu=0$, $W_\nu(\bar{\rho}^\nu)$ is a one-variable function and it takes a very short computation time in order to reach the bottom of the deepest valley of the one-dimensional curve. This becomes visually appreciable if a one-dimensional function with multiple valleys is plotted against a single variable on the abscissa. When $\nu=1$, the complexity of $W_\nu(\bar{\rho}^\nu)$ only increases twofold. When ν becomes large, although the structure of $W_\nu(\bar{\rho}^\nu)$ becomes very complex, it is not formidably time consuming for the test profile to move because the test profile has by now reached a position very close to the largest and deepest pit in the entire domain of $W_\nu(\bar{\rho}^\nu)$.

The motion of a test profile at a given stage ν is composed of many discrete moving steps. Each step can in principle be calculated by solving Newton's equation of motion (as in molecular-dynamics simulation). However, as in Monte Carlo atomistic simulation, it is also legitimate to use random numbers to generate the moves. The difference between solving the equation of motion and the use of random numbers is that only a fraction of the attempted moves are accepted for the latter, while the former uses all moves. The advantage to using the latter for our present purpose is that one can save computation times by skipping the enormous amount of work involved in the more time-consuming calculation of the force due to the derivatives [see Eq. (23)]. In (iii), we describe how to use random numbers to generate moves. There is a sampling cell which determines the size of the maximum region which the random sampling can cover. This size is designed to follow a decreasing sequence as the test profile moves along within a given stage ν. At the beginning of the stage, we want to jump from pit to pit in the entire domain of definition of $W_\nu(\bar{\rho}^\nu)$, so the sampling cell should be equal to the entire domain. But as the test profile becomes more localized, the sampling cell size is gradually reduced to focus on more important locations. The gradual reduction is called the downscaling of the sampling size and it is described in (iv). The downscaling is also needed after the test profile jumps into a particular pit. For a given number of samplings, a test profile can move faster toward, and hit more precisely on, the very bottom point of the pit if the sampling cell is scaled down synchronously to sufficiently small values at the end.

(iii) Monte Carlo construction of random move $\Delta\bar{\rho}^\nu$ for $\bar{\rho}^\nu$. A 2^ν-dimensional random vector is generated as follows:

$$\bar{R}^\nu = (R_1^\nu, R_2^\nu, \ldots, R_{2^\nu}^\nu) \tag{24}$$

$$-1 \le R_j^\nu \le 1 \ , \tag{25}$$

where R_j^ν is a random number uniformly distributed in the interval $(-1,1)$. The random number can be generated using a regular generator such as the ones available in [11] or the ones used in standard Monte Carlo simulations. This random vector $\bar{R}^\nu$ can be used to create a random move $\Delta\bar{\rho}^\nu$ in a sampling cell of diameter δ_q by

$$\Delta\bar{\rho}^\nu=\delta_q\bar{R}^\nu ,$$
$$\delta_q=\delta_0(1-p)^q , \tag{26}$$

where δ_q $(q=0,1,2,\ldots)$ forms a decreasing sequence which controls the diameter of the sampling cell, p is the percentage of reduction in each scaling, and $(1-p)$ is the scaling factor. At the beginning of the scaling, $q=0$, the diameter of the scaling cell δ_0 is equal to the maximum range of the SLD profile as determined in the following:

$$\delta_0=\rho_U-\rho_L , \tag{27}$$

where ρ_U and ρ_L denote, respectively, the upper and lower bounds of the SLD in the sample, and they are usually known for a sample composed of known constituents. The scaling factor $1-p$ can be determined by

$$p=\frac{1}{M}\sum_{i=1}^{M}\frac{\sigma_i}{|\mathcal{D}(k_{0i})|} . \tag{28}$$

This definition guarantees that the scaling is sufficiently slow such that a cell is properly sampled. The scaling sequence stops at $q=s$, such that

$$\frac{\delta_s}{\delta_0}\le p \quad \text{and} \quad \frac{\delta_{s-1}}{\delta_0}>p . \tag{29}$$

This enables the program to stop when the test profile essentially moves negligibly.

(iv) A sequential forward-backward walk alternative to the scheme in (iii). The scheme for generating a random move in (iii) is called a random number scheme. To this scheme, an alternative is to use a forward-backward walk. In this scheme, a move is generated by increasing or decreasing the value of a *single* component of the test profile vector $\bar{\rho}^\nu$. This move is equivalent to the test profile $\bar{\rho}^\nu$ making a walk forward or backward along a given axis. For a given component ρ_j, there are only two possibilities, one is an increase by a step size δ_q and the other a decrease by the same amount. This forward-backward move is applied to every component of $\bar{\rho}^\nu$ sequentially, but the sequence does not matter. When it has been applied to all the components once, the above sequential applications are repeated. The step size is defined by Eq. (26) and it is scaled down in the same way as described in (iii). This scheme was tested and found to be more efficient than the scheme in (iii).

(v) Newtonian motion $\Delta\bar{\rho}^\nu$ of $\bar{\rho}^\nu$ in the force field defined by Eq. (23). The move constructed in (iii) and (iv) may or may not be in accordance with Newton's law of motion. If it is the former, then the test profile moves forward. If it is the latter, the test profile should wait until another random move constructed by (iii) is judged to be in line with Newton's law of motion. Newton's law of motion states that the acceleration of a body is proportional to the force it undergoes, and the proportionality constant is a positive number called the mass of the body. Consequently, for a stationary body at time zero, the spatial displacement after a time lapse t is in the direction of the force and is equal to the product of the force and the squared time t^2 divided by twice the mass. In the present case of the motion of a test profile, the time t and mass m are not defined and are of no importance. We are interested in how the displacement $\Delta\bar{\rho}^\nu$ is related to the force $\bar{F}_\nu(\bar{\rho}^\nu)$ because this determines the locus of the test profile in the solution space. Therefore, we can express Newton's law of motion as applied to the time interval in which a given move is made as

$$\Delta\bar{\rho}^\nu=c\bar{F}_\nu(\bar{\rho}^\nu) \quad (c>0) , \tag{30}$$

where c is a positive constant. Equation (30) can be rewritten as

$$\frac{\bar{F}_\nu(\bar{\rho}^\nu)}{\Delta\bar{\rho}^\nu}=\frac{1}{c}>0 . \tag{31}$$

Since the random move can be a large step, especially in case of jumps, Eq. (23) is best written in the form of a difference equation,

$$\bar{F}_\nu(\bar{\rho}^\nu)=-\frac{W_\nu(\bar{\rho}^\nu+\Delta\bar{\rho}^\nu)-W_\nu(\bar{\rho}^\nu)}{\Delta\bar{\rho}^\nu} . \tag{32}$$

Substituting Eq. (32) into Eq. (31), we obtain

$$W_\nu(\bar{\rho}^\nu+\Delta\bar{\rho}^\nu)-W_\nu(\bar{\rho}^\nu)=-\frac{[\Delta\bar{\rho}^\nu]^2}{c}<0 . \tag{33}$$

Equation (33) is the final form of Newton's equation of motion for a discrete move $\Delta\bar{\rho}^\nu$ in the potential field $W_\nu(\bar{\rho}^\nu)$.

A move $\Delta\bar{\rho}^\nu$ constructed in (iii) and (iv) is considered a Newtonian move if it satisfies Eq. (33), and a non-Newtonian move otherwise. The Newtonian motion of the test profile in the potential field $W_\nu(\bar{\rho}^\nu)$ consists of one Newtonian move after another Newtonian move. When a Newtonian move is obtained the test profile moves into the new position and waits to make another Newtonian move. In this way, the test profile can move from the beginning of a stage ν to its end.

3. *Transition from stage ν to the next stage $\nu+1$*

When the Newtonian motion of the test profile is completed at stage ν, the test profile stops moving and a transition to the next stage $\nu+1$ is in order. During the transition, the number of dimensions of the new test profile $\bar{\rho}^{\nu+1}$ has increased through the delumping of the old lumped test profile $\Delta\bar{\rho}^\nu$. The increase is a doubling from 2^ν dimensions to $2^{\nu+1}$ dimensions. The lumping ratio of the test profile $\bar{\rho}^{\nu+1}$ is accordingly halved compared to that of $\bar{\rho}^\nu$. The transition needs to preserve the continuity of the test profile from $\bar{\rho}^\nu$ to $\bar{\rho}^{\nu+1}$. Fortunately, this can be very easily done because the lumping scheme in Sec. III D has already taken this factor into account. The transition is illustrated in the following.

At the end of stage $\nu=0$, the test profile $\bar{\rho}^0=(\rho_1^0)$ is recorded. This variable is a lumped pack of n variables.

We cut the N-variable lump into two halves; each is a lumped pack of $N/2$ variables. Then we have a two-variable vector $\bar{\rho}^1_{\text{in}}=(\rho^0_1,\rho^0_1)$ with two equal components and we set it to be the initial position of the test profile at the beginning of stage $\nu=1$. The test profile $\bar{\rho}^1$ makes Newtonian moves until the end of this stage and the final position $\bar{\rho}^1=(\rho^1_1,\rho^1_2)$ is recorded. Then the test profile is ready to make the transition to stage $\nu=2$. Since each of the two components of $\bar{\rho}^1$ is a lumped pack of $N/2$ dimensions, cutting it into halves of $N/4$ dimensions would create a vector of four components $\bar{\rho}^2_{\text{in}}=(\rho^1_1,\rho^1_1,\rho^1_2,\rho^1_2)$ from $\bar{\rho}^1$. We set this vector to be the initial position of the new test profile $\bar{\rho}^2$; then $\bar{\rho}^2$ is ready to start its Newtonian motion at stage $\nu=2$. This bisection method can be similarly applied at each transition.

F. Summary

In the following, we summarize Secs. III A–III E in a procedure of six steps to construct a SLD profile from a set of M reflectivity data. By following these steps, one can construct a final profile from M measured reflectivity data.

(1) The SLD profile of the measured sample $\rho(z)$ is represented by its model-independent discretized version $\bar{\rho}_N=(\rho_1,\rho_2,\ldots,\rho_N)$ as discussed in Sec. III A and then a so-called groove in the solution space is constructed by the lumped-dimensions method (see Sec. III D). This groove consists of $n+1$ stages or sections $\nu=0,1,2,\ldots,n$. It serves as a constraint to make $\bar{\rho}_N$ take the form of a test profile $\bar{\rho}^\nu$ which changes dimensions at different stages according to 2^ν as it moves from stage to stage.

(2) Depending on the specific sample, the profile $\bar{\rho}_N$ can be chosen to start moving from a specific starting stage ν_0 on the groove (ν_0 may be 0 or other values no greater than n), and the initial position at the starting stage ν_0 is chosen according to Sec. III E 1. At this stage, the groove constrains the profile $\bar{\rho}_N$ to take the form of a test profile $\bar{\rho}^{\nu_0}$ which has 2^{ν_0} dimensions (less than $N=2^n$).

(3) At the starting stage ν_0, $\bar{\rho}_N$ in the form of $\bar{\rho}^{\nu_0}$ begins to move away from a given initial position assigned in step (2). The motion is carried out according to Sec. III E 2. The way to do it is by generating a move $\Delta\bar{\rho}^{\nu_0}$ according to the schemes in (iii) or (iv) in Sec. III E 2, judge if it agrees with Newton's law of motion in the form of Eq. (33), and implement or reject this move depending on whether or not it satisfies Eq. (33), respectively. When the random number scheme in (iii) is used, this trial-judgment act is repeated until no move is accepted for L consecutive trials for L being statistically very large. If the walk scheme in (iv) is used, the trial-judgment act continues until none of the components of $\bar{\rho}^{\nu_0}$ is capable of moving any further.

(4) At completion of (3), the size of the sampling cell for generating $\Delta\bar{\rho}^{\nu_0}$ is scaled down according to Eq. (26), and (3) is repeated. When (3) stops again, the sampling cell is further scaled. The scaling continues until Eq. (29) is satisfied. At this point, the motion of the profile at stage ν_0 is considered completed.

(5) When (4) is completed, the profile makes a transition to stage ν_0+1 according to Sec. III E 3. At the new stage, the profile $\bar{\rho}_N$ takes the constrained form $\bar{\rho}^{\nu_0+1}$. The motion is carried out in the same way as at stage ν_0, namely, steps (3) and (4) are repeated.

(6) The three steps (3), (4), and (5) are repeated until the motion at the last stage $\nu=n$ is completed. Now, the profile has reached its final position, and its value is recorded as the constructed profile from the M data.

IV. APPLICATIONS OF METHOD TO SIMULATED REFLECTIVITY DATA

In this section we generate some reflectivity data using the Parratt's recurrence formula for a few SLD profiles which resemble the ones used in reflectivity experiments. Then we apply the method developed in Sec. III to these data and investigate whether or not said method can faithfully reconstruct the SLD profiles. The term "reconstruct" is used because in producing the M discrete reflectivity data via the Parratt's formula, an original SLD profile is cut into pieces and is turned into M discrete dimensionless numbers from which one wants to rebuild the SLD profiles.

The reason for using the simulated data is that the actual SLD profiles are known beforehand; thus, the correctness of the reconstructed profiles can be checked directly against the known profiles. In this way, the reliability of the method itself can be confirmed, and this serves as an indirect evidence that the SLD profiles reconstructed by the method from measured reflectivity data are correct. In the following, first, the simulated reflectivity data from an exponential profile (or the Cahn model) typical of polymer segregation at the air surface are inverted. Second, the method is applied to the simulated data from an error-function profile representative of interdiffusion between two materials. Lastly, an oscillatory profile resembling the surface structures of bicontinuous microemulsions is simulated, and the reflectivity data are inverted to reconstruct this profile. Although these profiles are not exhaustive, their functional behaviors do cover a wide range of complexities so that it is reasonable to say this method can reconstruct most SLD profiles met in real experiments if it can faithfully reconstruct the above profiles. Note that a Gaussian noise of a few percent is introduced into the simulated data in Secs. IV A–IV C to simulate experimental errors.

A. The Cahn model in polymer segregation

When deuterated polystyrenes segregate, the air-sample interface has a concentration profile described by the Cahn model

$$\phi(z)=\phi_\infty+(\phi_M-\phi_\infty)e^{-(z+d)/\lambda}, \tag{34}$$

where ϕ_M and ϕ_∞ are the volume fractions of deuterated polystyrenes at the air-sample interface and at ∞ into the bulk, respectively. If we choose the parameters $\phi_M=0.5$, $\phi_\infty=0.05$, and $\lambda=100$ Å, then the corresponding SLD profile would be

$$\rho(z)=1.67\times10^{-6}+2.22\times10^{-6}e^{-(z+d)/100}\ . \quad (35)$$

The dimension of $\rho(z)$ is Å^{-2}. The parameter d is the distance from the air-sample interface to the origin of the z coordinate and is chosen to be 1000 Å in this case.

Using the profile in Eq. (35), the reflectivity is generated by the Parratt's formula and is plotted in circles in Fig. 3(b). Applying the method of Sec. III to the data, we obtain a reconstructed profile as given by the solid line in Fig. 3(a). The actual profile is plotted in dashed line in the same graph. The reconstruction is faithful to the actual profile. The reflectivity of the reconstructed profile in Fig. 3(a) is calculated and plotted in solid line in Fig. 3(b). The comparison with the simulated data in Fig. 3(b) is within 3%. The conclusion from this example is that the method works on segregation profiles like the one in Fig. 3(a).

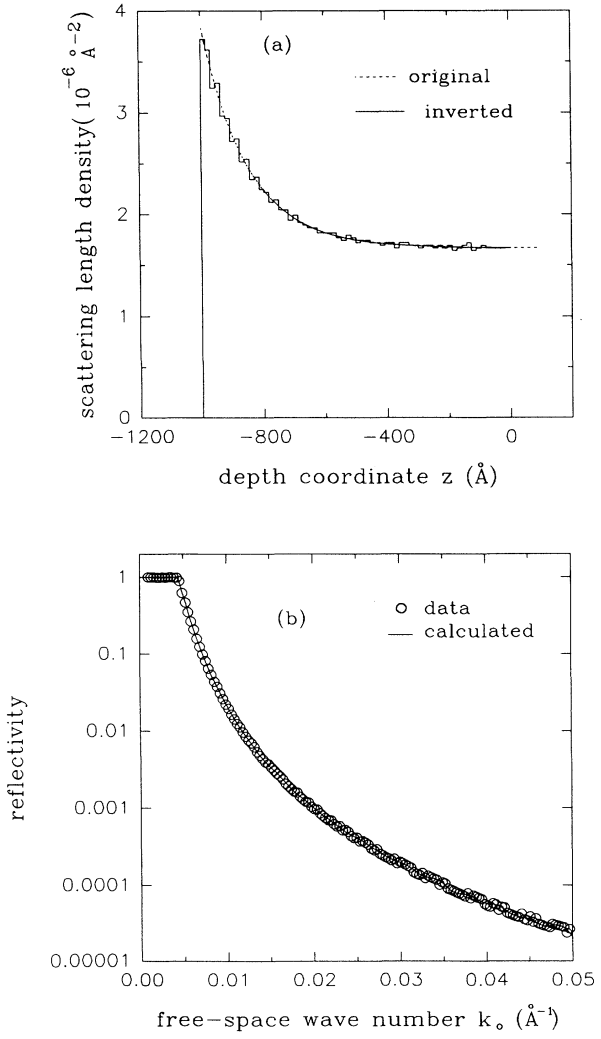

FIG. 3. Inversion of the simulated reflectivity data of an exponential profile given by Eq. (35). This profile is called the Cahn model. (a) presents the reconstructed profile (solid line) compared with the actual profile (dashed line). The profiles continuously merge into a uniform bulk of 1.67×10^{-6} Å^{-2}. (b) is the calculated reflectivity (solid line) of the reconstructed profile compared with the simulated data (circles).

B. Error-function model in Fickian diffusion between two material regions

In the study of the diffusion between two material regions of different densities such as between a protonated polystyrene layer and a deuterated polystyrene layer, the interface density profile would be an error function if the diffusion is assumed to follow Fick's Law. Although deviations from the error function may occur when the densities are very high or when constituents of the material regions cannot be approximated by small spherical particles, the error-function model is still important because it is representative of a class of density profiles resulting from a transition from one density level to another.

Suppose a 750-Å uniform layer of protonated polystyrene (HPS) is placed on top of a 750-Å uniform layer of deuterated polystyrene (DPS) which in turn is situated on top of a semi-infinite fused silica substrate. The neutron SLD densities are 1.43×10^{-6}, 6.4×10^{-6}, and 3.48×10^{-6} Å^{-2} for HPS, DPS, and fused silica substrate, respectively. Upon annealing for some time at a certain temperature, the two layers diffuse into each other and the interface region becomes a gradual sloping-up. If the diffusion is assumed to be Fickian, then the sloping-up profile would be an error function. Suppose the profile takes the following form:

$$\rho(z)=1.43\times10^{-6}+2.50\times10^{-6}\left[1+\text{erf}\left[\frac{z+750}{150}\right]\right]\ . \quad (36)$$

This profile is calculated and plotted in dashed line in Fig. 4(a). Note that in practice the reptation effect will cause the actual profile to deviate from the standard form in Eq. (36) [12].

The reflectivity of this profile is simulated using the Parratt's formula and the data are given in circles in Fig. 4(b). Applying the method in Sec. III to these simulated data, we obtained the reconstructed profile plotted in solid line in Fig. 4(a). Apparently, the reconstructed profile is in close agreement with the actual profile (within 2%). To further confirm the correctness of the profile, the reflectivity of this profile is calculated and plotted in solid line in Fig. 4(b) to compare with the simulated data. The reconstructed profile does give a reflectivity curve which is very close to the simulated data. Because the experimental profile is at least similar to the profile in Eq. (36) although it may not be exactly an error function, the effectiveness of this method as applied to the error-function profile in Eq. (36) gives one the confidence to apply it to real experimental data measured from an actual diffused profile. Besides the profile in Eq. (36), we have tried similar profiles with different parameters, substrates, and orientations with respect to the incident beam; in all cases, the original profiles have been faithfully reconstructed without exception.

C. Damped oscillatory surface profile

It was recently discovered that the surface of a bicontinuous microemulsion assumes a damped oscillatory form [5]. A close representation of this surface structure is the following function:

$$\rho(z)=\rho_b+(\rho_M-\rho_b)e^{-(z+d)/\xi}\frac{\sin[\kappa(z+d)]}{\kappa(z+d)}\ , \qquad (37)$$

where ρ_b is the bulk SLD density, ρ_M the maximum SLD value at the surface, ξ the correlation length, and $\kappa=2\pi/D$, with D denoting the domain-domain repeat distance [5]. For the present purpose, we choose the parameters $\rho_b=3.0\times10^{-6}$ Å^{-2}, $\rho_M=6.0\times10^{-6}$ Å^{-2}, $\kappa=\frac{1}{30}$ Å^{-1}, and $\xi=800$ Å. This profile is plotted in dashed line in Fig. 5(a). It is then used to generate simulated reflectivity data as given in circles in Fig. 5(b). Application of the method in Sec. III to the data results in a reconstructed profile plotted in solid line in Fig. 5(a). The reconstructed profile is very close to the actual profile. The reflectivity calculated from the reconstructed profile is plotted in solid line in Fig. 5(b) and it is seen to agree with the simulated data very well. This example is evidence that the method would work on oscillatory profiles in reflection experiments. Examples of successful applications to real experimental data can be found in [5].

In conclusion, the method developed in Sec. III can reconstruct faithfully the SLD profiles as discussed above. This means that it is reasonable to assume that it can be applied to experimental data from similar samples.

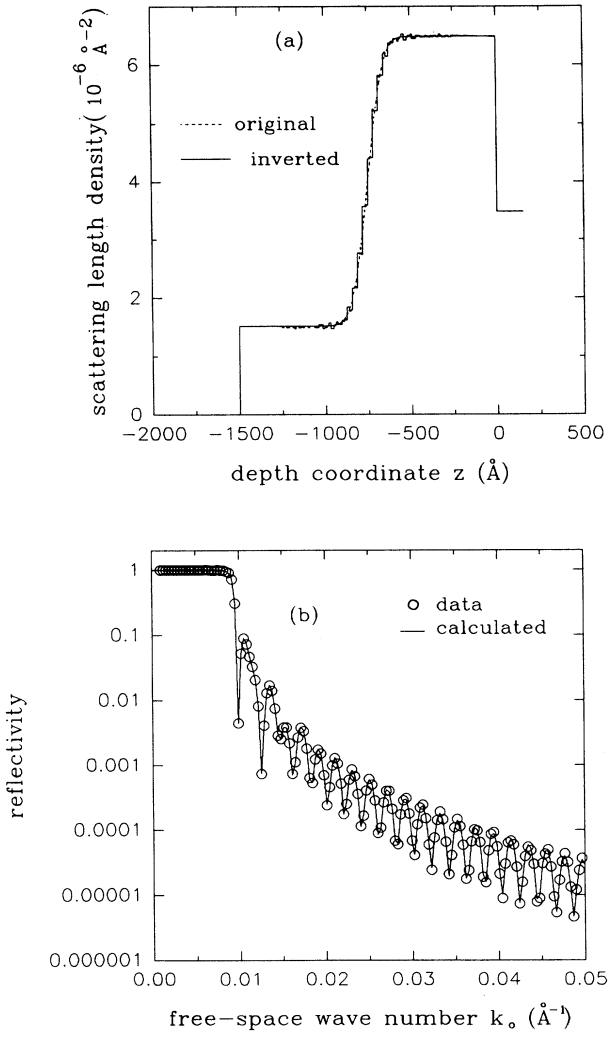

FIG. 4. Inversion of the simulated reflectivity data of an error-function profile given by Eq. (36). This profile follows from Fick's law in diffusion. (a) is the reconstructed profile (solid line) compared with the actual profile (dashed line). The substrate is fused silica of SLD $\rho_s=3.48\times10^{-6}$ Å^{-2}. (b) displays the calculated reflectivity (solid line) of the reconstructed profile compared with the simulated data (circles).

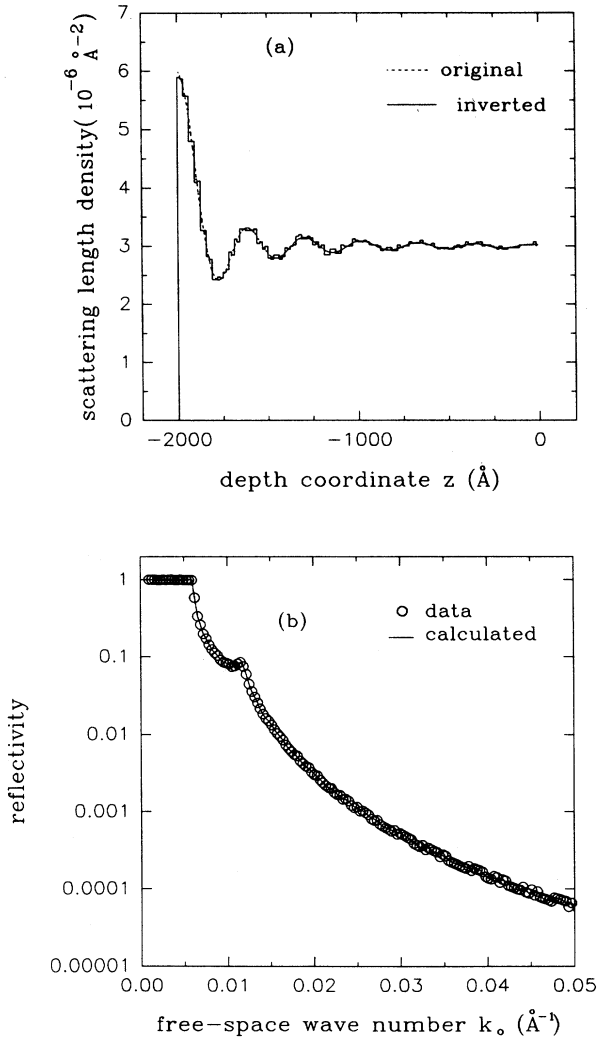

FIG. 5. Inversion of the simulated reflectivity data of a damped oscillatory profile given by Eq. (37). This profile resembles the surface structure of a bicontinuous microemulsion. (a) presents the reconstructed profile (solid line) compared with the actual profile (dashed line). The bulk has a SLD of 3.0×10^{-6} Å^{-2}. (b) is the calculated reflectivity (solid line) of the reconstructed profile compared with the simulated data (circles).

V. APPLICATIONS OF METHOD TO MEASURED REFLECTIVITY DATA

In this section we present some applications of the method to the inversion of measured reflectivity data. The reflectivity data to be used are from three different types of samples: an AOT-D_2O-oil microemulsion surface, a diffused polymer-polymer interface, and two end-functionalized polymer samples exhibiting surface adhesions [AOT is sodium bis(2-ethylhexyl)sulfosuccinate]. In the following, we describe in detail the three experiments and the analysis of the data using the method in Sec. III. In essence, this section is a viability test of the method under practical circumstances.

A. Surface structure of microemulsion D_2O-decane-AOT of $\alpha=40$, $\gamma=20$ at $T=25.2$ °C

In [5], three sets of measured reflectivity data from bicontinuous $C_{10}E_4$-D_2O-octane microemulsions were inverted using the same method as presented in Sec. III to produce the SLD structures at the air-microemulsion interfaces. It was discovered for the first time that the surface regions were layered due to the presence of the surface. For the purpose of illustration of the method in such applications, we present here the reconstruction of the surface SLD structure of another microemulsion consisting of AOT, D_2O (brine), and decane. The parameters of this microemulsion are $\alpha=40$, $\gamma=20$, and $T=25.2$ °C. Note that the SLD values for the three components are 0.593×10^{-6}, 6.38×10^{-6}, and -0.487×10^{-6} Å^{-2}, respectively.

A neutron reflectivity experiment was performed on this sample at the reflectometer at Saclay, France. For the procedures and precautions used in this experiment, the reader is referred to the description in [5]. The data are shown in circles in Fig. 6(b). Using the method in Sec. III to these data, we have obtained a surface profile plotted in solid line in Fig. 6(a). It is found that this microemulsion, like $C_{10}E_4$-D_2 O-octane, also exhibits an oscillatory surface density structure. The physics behind this phenomenon is expected to be the same as for $C_{10}E_4$-D_2O-octane. Since the main purpose of this example is to illustrate the practical applications of the method, we do not intend to discuss the detailed physics of this sample; instead we refer the reader to [5] for more information in this respect.

The reflectivity of the reconstructed profile in Fig. 6(a) is calculated using the Parratt's formula and is plotted in solid line in Fig. 6(b) for comparison with the measured data. The agreement is within 3%. Aided by the application of the method to the simulated reflectivity data from a similar oscillatory profile in Sec. IV C, we are confident that the reconstructed profile in Fig. 6(a) is correct and reflects the actual surface structure of the microemulsion.

B. Diffused interface profile of HPS-DPS bilayer

In Fig. 7(b) are plotted the reflectivities as a function of k_0. The circles represent the measured reflectivity by Felcher, Karim, and Russel [12] from a polymer bilayer on a silicon substrate. Before the experiment, the sample was a 850-Å-thick DPS layer put on the top of a 5000-Å-thick HPS layer on a silicon substrate. Then it was annealed to induce interdiffusion. Before annealing, the DPS layer and the HPS layer have a constant scattering-length density of 6.3×10^{-6} and 1.43×10^{-6} Å^{-2}, respectively. After annealing for 15 min at 155 °C, the two layers diffused into each other, so the boundary between them became more gradual. The detailed structure of the density profile reflects the physical processes responsible for diffusion. The measured neutron reflectivity data in Fig. 7(b) (circles) are inverted with the method described in Sec. III to yield the profile in Fig. 7(a) (solid line). In this figure, the region $z<-5850$ Å is air and the omitted portion of the HPS layer (the SLD is 1.43×10^{-6} Å^{-2}) extends to $z=0$, where it comes in contact with the sil-

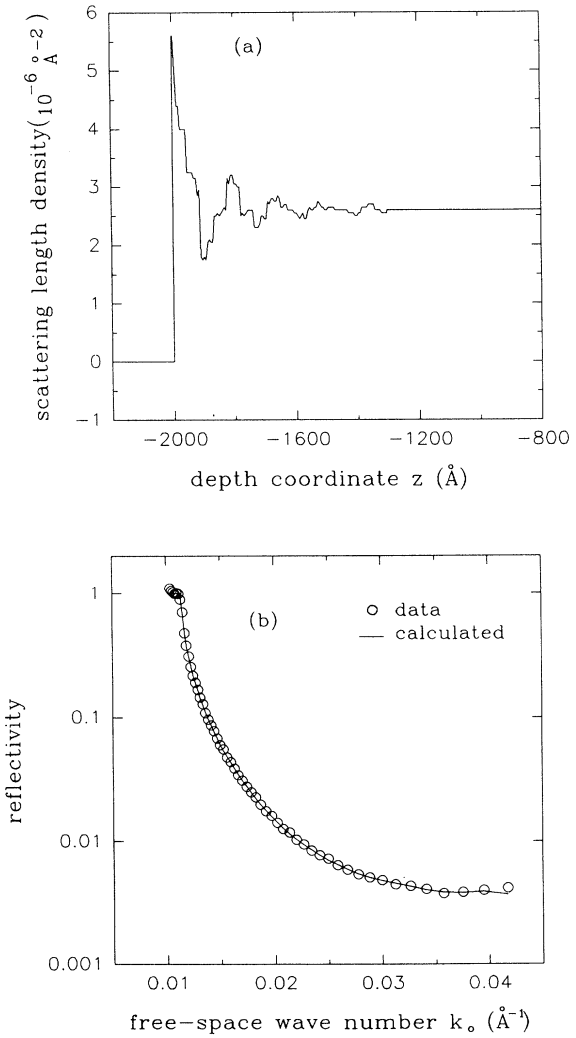

FIG. 6. Inversion of the reflectivity data measured from a microemulsion sample consisting of oil-D_2O-AOT at $\alpha=40$, $\gamma=20$, and $T=25.2$ °C. The sample is in the one-phase region in its phase diagram. (a) is the reconstructed profile (solid line). The bulk has a SLD of 2.60×10^{-6} Å^{-2}. (b) is the calculated reflectivity (solid line) of the reconstructed profile compared with the measured data (circles).

icon substrate. The interfacial density gap due to reptation as discussed in [12] is observed in this figure. To verify the validity of this inverted profile, its reflectivity is calculated against k_0 and plotted with solid line in Fig. 7(b). It follows the measured data very closely. Note that the SLD profile deviates from an error-function profile due to the reptation effect.

C. Adhesion properties of end-functionalized polymers

It has been contemplated that the neutron reflectivity experiments could determine the effect of the end groups on the surface adhesion properties of polymers. Experiments were carried out on samples consisting of uniform mixtures of polystyrenes. Seventy-five percent of each polystyrene chain is protonated, while 25% of the chain is deuterated. Then the deuterated end of the chain is terminated with a lithium or fluorine tip. The samples are situated on top of silicon substrates of SLD 2.08×10^{-6} Å^{-2}. Since the sample is a uniform mixture, obviously, the only places where structures can occur are the air surface and the substrate surface. The middle of the samples should be uniform bulk. For a given chain at the surface, the terminated deuterated end could either be drawn to the surface or remain unaffected by the presence of the surface. The former would result in a high SLD density region next to the surface followed by a low SLD density region corresponding to the protonated segment of the chains. Note that the high-density region

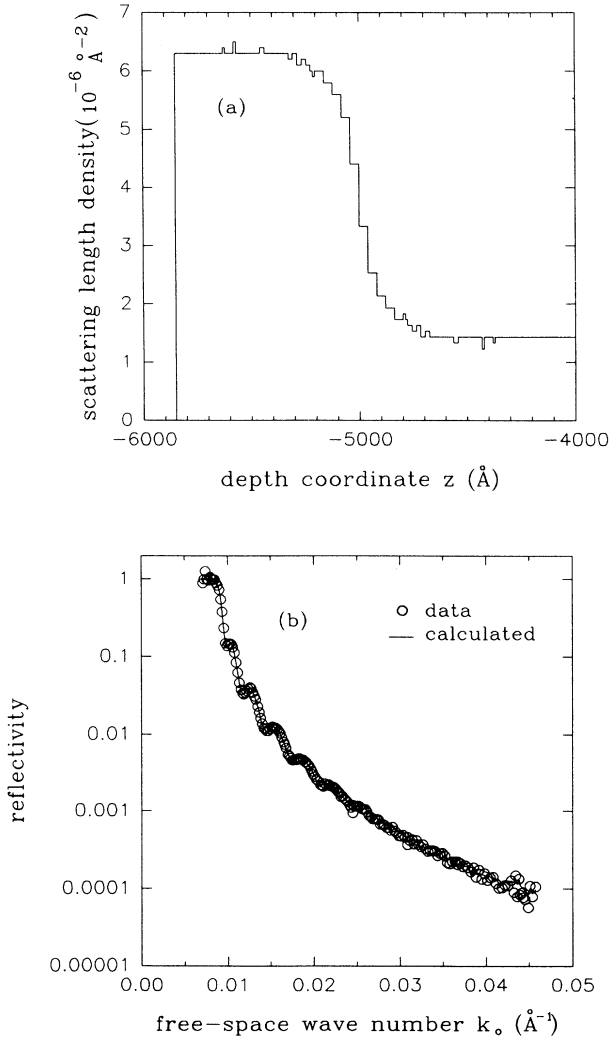

FIG. 7. Inversion of the reflectivity data measured from a diffused interface between a DPS layer of 850 Å and a HPS layer of 5000 Å. The substrate is silicon of 2.08×10^{-6} Å^{-2}. The sample was annealed at 155 °C for 15 min to induce diffusion. (a) gives the reconstructed profile (solid line). (b) gives the calculated reflectivity (solid line) of the reconstructed profile compared with the measured data (circles).

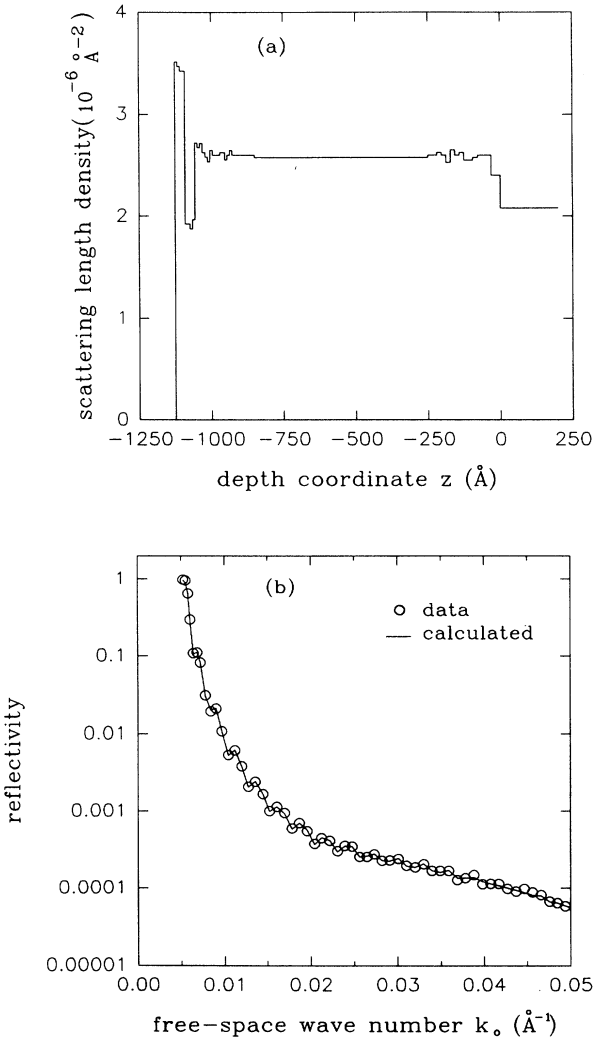

FIG. 8. Inversion of the reflectivity data measured from a 1125-Å-thick polymer sample consisting of a mixture of polystyrene chains. Each chain has 75% of its length protonated and 25% of its length deuterated, and the latter is terminated with a fluorine tip. This sample was annealed at 110 °C for 16 h to induce adsorption. The substrate is silicon of 2.08×10^{-6} Å^{-2}. (a) presents the reconstructed profile (solid line). (b) gives the calculated reflectivity (solid line) of the reconstructed profile compared with the measured data (circles).

could be considerably wider than the length of the deuterated segment as the polymers are tangled together. The latter would lead to a uniform region near the surface. The neutron reflectivity experiments are supposedly able to detect whether the former or the latter is the case at both the air and the substrate surfaces. More than 20 sets of experimental data were obtained by Dr. J. Koberstein *et al.* (University of Connecticut) at the POSY reflectometer at IPNS, Argonne National Laboratory. However, the lack of a model-independent method to reconstruct the SLD profiles from the data has prohibited successful processing of the data. With the development of the method in Sec. III, we have successfully reconstructed the profiles from some of these data given to us by Dr. Koberstein. In the following, we present two examples to demonstrate the power of this method.

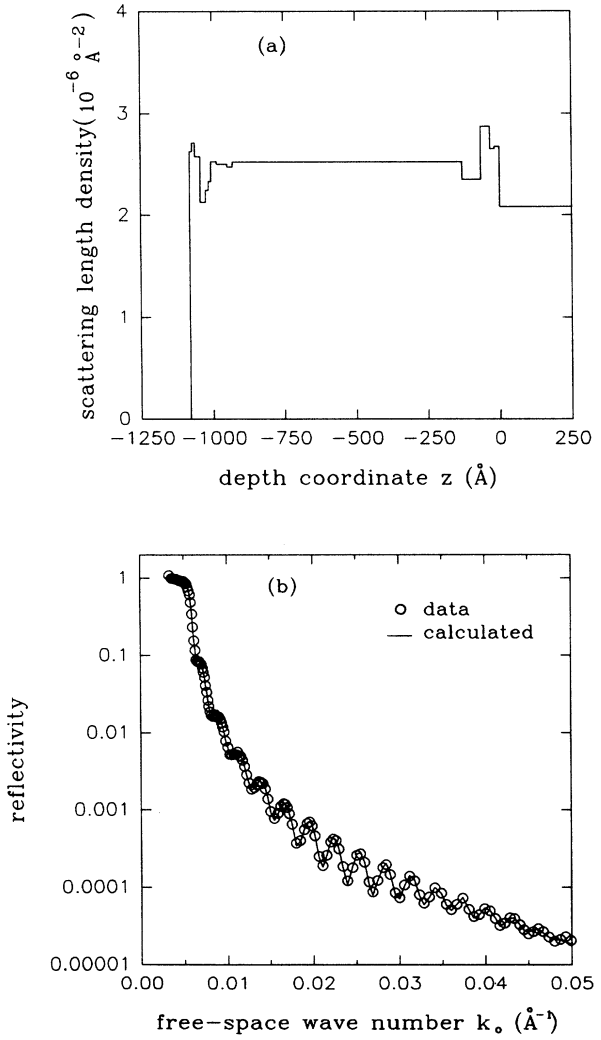

FIG. 9. Inversion of the reflectivity data measured from a 1050-Å-thick polymer sample consisting of a mixture of polystyrene chains. Each chain has 75% of its length protonated and 25% of its length deuterated, and the latter is terminated with a lithium tip. The sample was annealed at 110 °C for 16 h to induce adsorption. The substrate is silicon of 2.08×10^{-6} Å^{-2}. (a) gives the reconstructed profile (solid line). (b) gives the calculated reflectivity (solid line) of the reconstructed profile compared with the measured data (circles).

The first set of data were measured from a polystyrene sample with fluorine termination. The data are plotted in circles in Fig. 8(b). The reconstructed profile is given in solid line in Fig. 8(a). In obtaining the profile, the middle of the profile was constrained to be constant to save computation time. It is seen that there is a high-density layer at the front surface. This indicates that the fluorine tip has the effect of adhesion to the air surface. The correctness of the profile is confirmed by comparing the calculated reflectivity of the profile as given by the solid line in Fig. 8(b) with the data shown by circles in the same graph. Note that the high-density layer in the front is followed by a layer of low-density region.

The second set of data were from a polystyrene sample with lithium termination. The data are given in circles in Fig. 9(b). The reconstructed profile is plotted in solid line in Fig. 9(a). It indicates the occurrence of adhesion at both the air and silicon surfaces. This seems to mean that lithium has an affinity to silicon as well as to air. The calculated reflectivity of this profile is plotted in solid line in Fig. 9(b). It is in good agreement with the measured data.

VI. DISCUSSION

A model-independent method for reconstructing the SLD profile from a set of M reflectivity data has been developed and successfully tested on both simulated and measured data. It is model independent because no preassumed SLD profile models are needed in order to carry out the reconstruction calculation. For example, the damped oscillatory structures in the surface region of the microemulsion sample shown in Sec. V A had not been known before a direct application of the method given in Sec. III to the measured reflectivity data. The reconstruction calculation unexpectedly produced such a structure. In the inversion process using the method of Sec. III, the surface region was discretized into 256 small segments and the SLD values of all 256 segments were self-consistently generated from the M reflectivity data such that the calculated reflectivity of the final profile agreed with the measured reflectivity data to within the error bars of the data. The oscillatory form of the reconstructed profile had not been preassumed; therefore, the method is truly model independent. In addition, for N sufficiently large, such a discretized profile of N segments can represent most SLD profiles in a practical reflectivity experiment. Therefore, the method is capable of reconstructing SLD profiles of both discrete and continuous functional forms free of preassumed models. However, this does not exclude the possibility of incorporating known constraints about a sample into the inversion process. In fact, this can be very easily done. One example is the use of a uniform bulk constraint on the middle section of the adhesion sample in Sec. V C. Another example is the use of the knowledge about the symmetry of the diffused interface in Sec. V B.

In the implementation of the method, the thickness parameter d is largely a free choice as long as it is larger

than the actual thickness of the sample. It should be large enough to include the entire film (excluding the substrate) within the spatial region $(-d,0)$ so that no SLD structure is lost. This requirement can be satisfied in three ways: (1) If the actual thickness d_a of the film is accurately known beforehand, then d is set to d_a; (2) if d_a is only known approximately, then a conservative estimate of the maximum possible value of d_a should be used for d; and (3) if nothing is known about the thickness of the film, one can always use the maximum sensitive depth d_s of the probing beam as the value of d. The sensitive depth d_s is defined as the depth beyond which the SLD structures cannot be detected by a reflectivity measurement. It can be estimated from the experimental resolution Δk_0. In order to sensitively detect the existence of an interface situated at d_s from the air-film interface, the reflectivity curve should preserve the oscillating features due to the interference between the reflection from the interface at d_s and that from the air-film interface. This means that there should be at least two data points within each half-period of the oscillation. Since the minimum distance between two data is Δk_0, this condition requires that $d_s=\pi/2\Delta k_0$. This formula can be applied to both x rays and neutrons. For a neutron reflection experiment, suppose the uncertainty in k_0 is $\Delta k_0/k_0=3\%$. This gives $\Delta k_0=6\times10^{-4}$ Å^{-1} at $k_0=0.02$ Å^{-1}, a typical value. Then the sensitive depth is calculated to be $d_s\approx2600$ Å. To be more conservative, one may relax the requirement of two data points per half-period to one datum per half-period. In this case, the sensitive depth is determined by $d_s=\pi/\Delta k_0$. According to this condition, the sensitive depth becomes $d_s\approx5200$ Å. Using d_s as d, one is assured that the detectable region of the SLD profile is effectively included in the interval $(-d,0)$. In practice, case (2) is more common than cases (1) and (3). For example, if the thickness of a polymer sample can be determined by ellipsometry to a precision of 30%, one may let the value of d equal 1.3 times the thickness determined by ellipsometry, and this d is sufficient to contain the whole film in $(-d,0)$. To be more conservative, one can even use 1.5 times the ellipsometric thickness as the value of d. Once a conservative d is chosen as discussed above, then the method in Sec. III will automatically make the value of the reconstructed SLD profile in the extra region of $d-d_a$ adjacent to air zero, or, alternatively, it will make the reconstructed SLD profile in the extra region of $d-d_a$ facing the substrate identical to the substrate. In this way, the real thickness of the profile is correctly recovered by the method.

Another issue is the number of segments N within the total thickness d. It is essentially determined by the spatial resolution of the probing beam. This resolution is comparable to the wavelength of the wave. For neutrons, the resolution is a few angstroms (say, 10 Å), and for x rays it is about one angstrom. For example, for $d=1000$ Å in neutron reflection, N should be 100 in order to make the pixel size of the profile comparable to the spatial resolution of the probing wave. For typical neutron experiments, since the sensitive depth is a few thousand angstroms, N is about a few hundred. This number of pixels can be handled very efficiently by our method on a regular workstation such as a DEC 5000 or an IBM 6000.

In an experiment, there is an uncertainty in the k_0 value and it is defined as the $\Delta k_0/k_0$ factor. It is about a few percent (say, 2% to 10%) for neutron experiments and is less than 1% for x rays. The measured reflectivity is considered as an average of the reflectivity over a range of exact k_0 values weighted by a Gaussian distribution with a standard deviation Δk_0. In the method in Sec. III, this factor is routinely implemented. The effect of this factor is the smearing of high-frequency variations and it is most significant at larger k_0 values. For example, the interference between the reflected wave from the front surface and that from the back surface would produce some fast oscillations in the reflectivity curve if the sample is thick, but one may not be able to see them in the measured reflectivity data due to the smearing effect of the uncertainty in k_0.

The roughness of surfaces are very common in practical samples. Since it has the effect of decreasing the effective Fresnel reflectance of an interface in the same way as a slope does to a sharp interface, it is accounted for in the method by automatically making a rough surface look like an interface with a slope. A flatter slope signifies a rougher surface, while a steeper slope indicates a smoother surface. By this token, the roughness parameter is not directly involved in the method. In neutron reflection experiments, since the spatial resolution is a few angstroms, a roughness of rms height of a few angstroms usually cannot be detected by reflection. Therefore, one should be careful in making conclusions about the roughness of a surface from neutron reflection data. A general caution is that arbitrary adjusting of the roughness parameter using the Debye-Waller factor in order to obtain good model fitting may lead to an artificial result.

The last factor in reflection is the absorption due to the imaginary part of the SLD. The imaginary part of the neutron SLD is discussed in [13]. For x-ray reflection, the imaginary part of the SLD can be found in [14]. In the present method, absorption is incorporated in the program, but it has been negligible in the examples considered for neutron reflection.

The method in Sec. III has been developed for the processing of neutron and x-ray reflectivity data, although all examples used are from neutron reflection. Also it is applicable to the inversion of reflectance data. We have tested the method on simulated reflectance data from more than 20 profiles and the result has been positive without exception. As a final word, it should be pointed out that successful applications of this method to other actual experiments depend on correct understanding of the sample and the interactions between the beam and the sample. It is advisable that constraints based on correct prior knowledge of the sample be beneficially used to save computation time and eliminate possible artifacts, and, lastly, that any reconstructed profile be scrutinized before conclusions are drawn.

ACKNOWLEDGMENTS

Xiao-Lin Zhou acknowledges financial support by the Argonne National Laboratory, by DOE, and by Schlum-

berger Research. Research work of Sow-Hsin Chen is supported by a grant from the Materials Science Division of DOE. The authors would like to thank Dr. Lay-Theng Lee for permission to use the data on the microemulsion D_2O/decane/AOT used in Sec. V A, Dr. A. Karim for providing the reflectivity data of the diffused polymer sample used in Sec. V B, and Dr. J. Koberstein for supplying the data of two adsorbed polymer samples used in Sec. V C. The authors would also like to thank Dr. Gian P. Felcher for many useful discussions about the validity and utility of the method developed in this paper and for his effort in giving a critical reading of this manuscript and diagnosing and test-running the computer code for data inversion on simulated reflectivity data at Argonne National Laboratory.

[1] T. P. Russel, Mater. Sci. Rep. **5**, 57 (1990).
[2] G. P. Felcher, Thin Film Neutron Optical Devices SPIE **983**, (1988).
[3] J. Penfold, Physica B **173**, 5 (1991).
[4] K. Kjaer and J. Als-Nielsen, Thin Solid Films **159**, 17 (1988).
[5] Xiao-Lin Zhou, Lay-Theng Lee, Sow-Hsin Chen, and R. Strey, Phys. Rev. A **46**, 6479 (1992).
[6] R. G. Netwon, in *Proceedings of Conference on Inverse Scattering: Theory and Applications,* edited by J. B. Bednar (SIAM, Philadelphia, 1983), pp. 1–74.
[7] T. M. Roberts, Physica B **173**, 157 (1991).
[8] Xiao-Lin Zhou, Sow-Hsin Chen, and G. P. Felcher, in *Inverse Problems in Scattering and Imaging,* edited by M. Bertero and E. R. Pike (Hilger, Bristol, 1991), pp. 109–130.
[9] B. E. Warren, *X-Ray Diffraction* (Addison-Wesley, Reading, MA, 1969).
[10] G. Parratt, Phys. Rev. **95**, 359 (1954).
[11] Julien C. Sprott, *Numerical Recipes* (Cambridge University Press, New York, 1991).
[12] G. P. Felcher, A. Karim, and T. P. Russel, J. Non-Cryst. Solid **131-133**, 703 (1991).
[13] V. F. Sears, Thermal-Neutron Scattering Lengths and Cross Sections for Condensed-Matter Research, Atomic Energy of Canada Limited Technical Report No. AECL-8490, 1984 (unpublished).
[14] A. H. Compton and S. K. Allison, *X Rays in Theory and Experiment* (Van Nostrand, New York, 1935), p. 279.